Coherent effects induced by static and time-dependent electric fields in semiconductors

T. Meier, G. von Plessen, P. Thomas, and S.W. Koch

Department of Physics and Materials Sciences Center, Philipps University, D-35032 Marburg, Germany
(Received 6 September 1994; revised manuscript received 6 February 1995)

Coherent effects are analyzed that are induced by homogeneous electric fields in photoexcited semiconductors. Extended semiconductor Bloch equations are presented, which include the applied electric field, in addition to the many-body Coulomb contributions in the time-dependent Hartree-Fock approximation. These equations are solved for a one-dimensional tight-binding model of a semiconductor superlattice. Linear and nonlinear optical signals associated with the coherent field-induced effects are calculated. For the case of a static electric field, the influence of the Coulomb interaction, which is treated on the Hartree-Fock level for a contact potential approximation, on the Bloch oscillations, and on their counterpart in the frequency domain, the Wannier-Stark-ladder, is analyzed. For a time-dependent electric field, dynamic localization, i.e., the localization of electrons due to an oscillating electric field, is analyzed. It is predicted that the dynamic localization should be observable in semiconductor superlattices even in the presence of Coulomb interaction.

I. INTRODUCTION

Recently, coherent effects induced by static electric fields in photoexcited semiconductors have received considerable interest. Examples include the field ionization of excitons,[1] virtual photoconductivity,[2] electric-field-induced optical rectification at semiconductor surfaces,[3,4] the ballistic acceleration of photoinjected electron-hole pairs,[5] and Bloch oscillations (BO) in semiconductor superlattices.[6,7] In this paper we present a theoretical approach to the coherent dynamics of photoexcited semiconductors in the presence of a homogeneous applied electric field. Our analysis includes the Coulomb interaction, which is known to play a dominant role in optical excitations close to the band edge.[8] While the linear optical properties of photoexcited semiconductors in the presence of static electric fields and Coulomb interaction are relatively well understood, theoretical treatments of the nonlinear field-induced coherent effects have either neglected the Coulomb interaction altogether,[4,9] or re-

stricted themselves to specific aspects of the excitonic problem.[2] We start from the well-known semiconductor Bloch equations (SBE's),[8,10] which have been used successfully to describe a number of linear and nonlinear coherent optical experiments in semiconductors without an applied electric field.[8,11] Recently, we have extended the SBE's to include also an applied electric field.[12] The solution of these extended SBE's allows the consistent calculation of coherent linear and nonlinear optical effects in semiconductors in the presence of homogeneous static or time-dependent electric fields. We have used these equations to demonstrate that, due to the combined influence of the Coulomb interaction and a static electric field, the interband polarizations and the populations can show different dynamic features, resulting in different oscillation times of the corresponding optical signals.[12]

The extended SBE, i.e., the equations of motion for the interband polarization $p(\mathbf{k}, t)$ and the populations $n_{c,v}(\mathbf{k}, t)$ in the conduction and the valence band, are given by[12]

$$\left[\frac{\partial}{\partial t} - \frac{e}{\hbar}\mathbf{F}(t) \cdot \nabla_{\mathbf{k}} - \frac{i}{\hbar}[e_c(\mathbf{k}, t) - e_v(\mathbf{k}, t)]\right] p(\mathbf{k}, t) = \frac{i}{\hbar}[n_c(\mathbf{k}, t) - n_v(\mathbf{k}, t)]\Omega(\mathbf{k}, t) + \left.\frac{\partial p(\mathbf{k}, t)}{\partial t}\right|_{\text{coll}},$$

$$\left[\frac{\partial}{\partial t} - \frac{e}{\hbar}\mathbf{F}(t) \cdot \nabla_{\mathbf{k}}\right] n_c(\mathbf{k}, t) = \frac{-2}{\hbar}\text{Im}\left[\Omega(\mathbf{k}, t)p^*(\mathbf{k}, t)\right] + \left.\frac{\partial n_c(\mathbf{k}, t)}{\partial t}\right|_{\text{coll}}, \qquad (1)$$

$$\left[\frac{\partial}{\partial t} - \frac{e}{\hbar}\mathbf{F}(t) \cdot \nabla_{\mathbf{k}}\right] n_v(\mathbf{k}, t) = \frac{2}{\hbar}\text{Im}\left[\Omega(\mathbf{k}, t)p^*(\mathbf{k}, t)\right] + \left.\frac{\partial n_v(\mathbf{k}, t)}{\partial t}\right|_{\text{coll}}.$$

<u>51</u>   14 490

Here $\mathbf{F}(t)$ denotes the homogeneous electric field, $e_c(\mathbf{k},t) = \epsilon_c(\mathbf{k}) - \sum_{\mathbf{k'}} V(\mathbf{k},\mathbf{k'})n_c(\mathbf{k'},t)$, $e_v(\mathbf{k},t) = \epsilon_v(\mathbf{k}) - \sum_{\mathbf{k'}} V(\mathbf{k},\mathbf{k'})n_v(\mathbf{k'},t)$ are the Coulomb-renormalized energies of electrons and holes, respectively, $\epsilon_c(\mathbf{k})$, $\epsilon_v(\mathbf{k})$ are the single particle energies, which are determined by the band structure. $\Omega(\mathbf{k},t) = \mu E(t) + \sum_{\mathbf{k'}} V(\mathbf{k},\mathbf{k'})p(\mathbf{k'},t)$ is the generalized Rabi frequency; μ is the dipole matrix element, $E(t)$ is the classical optical field, and $V(\mathbf{k},\mathbf{k'})$ is the Coulomb interaction. The terms given explicitly in Eqs. (1) are obtained in time-dependent Hartree-Fock approximation.[8] The subscript coll refers to many-body collision terms beyond the Hartree-Fock approximation, and to other dephasing mechanisms, such as carrier-phonon scattering.

Equations (1) are a direct generalization of the SBE to which they reduce for $F = 0$. In the derivation of these equations field-induced changes of the band structure[13] and Zener transitions between conduction and valence band[14,15] have been neglected, which is well justified for not too strong electric fields. In Eqs. (1) the electric field induces partial derivatives with respect to the quasimomentum. The dynamics induced by the accelerating electric field can be treated exactly, by introducing a moving coordinate frame through $\tilde{t} = t$, $\tilde{\mathbf{k}} = \mathbf{k} + \frac{e}{\hbar}\int^t \mathbf{F}(t')dt'$.[16] In this coordinate frame the partial derivatives with respect to the quasimomentum disappear and Eqs. (1) become formally equivalent to the SBE for the field-free case, with the additional condition that the quasimomentum obeys the so-called acceleration theorem $\frac{\partial}{\partial t}\tilde{\mathbf{k}} = \frac{e}{\hbar}\mathbf{F}$.[17]

In the numerical part of this paper we analyze the influence of the Coulomb interaction on the BO and their counterpart in the frequency domain, the Wannier-Stark ladder (WSL). Although both phenomena have been postulated a long time ago,[17,18] they have only recently been observed in semiconductor superlattices.[6,7,19] In semiconductor superlattices the requirement for the observation of both the WSL and the BO, i.e., that the scattering times must be larger than the BO time $T_B = \frac{h}{eFd}$ (F is the electric field amplitude and d the lattice constant), is much easier to fulfill than in bulk semiconductors. This is mainly due to the larger periodicity length (well plus barrier thickness) in the growth direction of superlattices compared to the atomic unit cell in bulk semiconductors. In superlattices the layer thickness is a design parameter which is determined by the growth conditions. The increased periodicity length leads to smaller BO times, which for experimentally realizable electric fields can become smaller than the coherence destroying carrier scattering times.

In this paper we describe the semiconductor superlattice using a one-dimensional tight-binding model.[9,16,19,20] For the Coulomb interaction we assume an on-site interaction, which retains the most important excitonic features, namely, a single bound excitonic state and an ionization continuum. Within this model we calculate the nonlinear signals which have been used to observe BO directly in the time domain, i.e., four-wave mixing (FWM) and terahertz (THz) emission signals. For the FWM signal we show that the Coulomb exchange interaction gives the dominant contribution to the sig-

nal, as in the case without applied electric field.[21] The linear spectra of superlattices in an electric field have been analyzed by Dignam and Sipe,[22] within a full three-dimensional model including excitonic effects. A discussion of the linear spectra obtained within our superlattice model, including analytical results, is given in the Appendix. Qualitatively the features of the calculated spectra agree with the results of Dignam and Sipe.

In the last part of this paper we calculate linear spectra and the THz emission for the case that an oscillating electric field is applied to the superlattice. We show that the dynamic localization,[16,23] i.e., the localization of electrons induced by an oscillating electric field, should be observable in the presence of Coulomb interaction. As a result of our calculations we predict that the dynamic localization should be observable in semiconductor superlattices using THz emission spectroscopy.

II. SEMICONDUCTOR SUPERLATTICE MODEL

The model which we use in the following is a one-dimensional tight-binding model of a semiconductor superlattice with cosine miniband dispersions for the electron and the heavy-hole minibands.[9,16,19,20] The collision terms in the extended SBE, Eqs. (1), are treated as simple exponential relaxation rates, with times T_1 and T_2 for the populations and the polarizations, respectively.[24] We assume on-site Coulomb interaction, i.e., $V(k,k') = V$. This form of the Coulomb interaction retains the most important excitonic features, namely, a single bound excitonic state and an ionization continuum.[25] Our model has the advantage of simplicity and great computational convenience; while it will not be capable of making rigorous quantitative statements, it does give qualitatively meaningful results.

With the contact Coulomb potential the momentum summations which appear in the modified SBE, Eqs. (1), reduce to

$$\sum_q V_{k-q}p(q) \Longrightarrow V\sum_q p(q) = Vp(r = 0),$$

$$\tag{2}$$

$$\sum_q V_{k-q}n_{c,v}(q) \Longrightarrow V\sum_q n_{c,v}(q) = Vn_{c,v}(r = 0) \quad.$$

Within this model the renormalization of the energies and the optical field, which are induced by the Coulomb interaction, are proportional to polarizations and populations at $r = 0$, with r being the relative coordinate between two carriers.

Within our two-band model we also neglect effects due to energetically higher minibands. This is justified for the case of static electric fields of the strengths we use in our numerical evaluations, as was shown by Bouchard and Luban.[26] They have solved the Schrödinger equation with an applied electric field for the parameters of the superlattice used in the experimental observation of the BO by Feldmann et al.[6] They find that transitions to higher minibands are not significant for times smaller than about ten BO times T_B, which is much larger than the dephasing time T_2 that sets an upper limit to the

experimentally observable time period. Also calculations of the interminiband scattering rates by Sibille[27] show that for not too strong electric fields the interminiband scattering rate is smaller than the dephasing rate and can therefore in good approximation be neglected. For time-dependent fields $\mathbf{F}(t)$ the same should be true if additionally the frequency of $\mathbf{F}(t)$ is not in resonance with an interminiband transition.

In the following we will, on the basis of this model, present calculations of various optical signals. For the case of a static electric field applied to the superlattice we discuss the FWM and THz emission signals. In the Appendix the linear spectra are discussed.

For the case of an oscillating electric field we study the dynamic localization under the influence of Coulomb interaction. In these calculations we use the following typical parameters for semiconductor superlattices: $\Delta = 20$ meV for the combined miniband width of the conduction and the valence minibands, $V = 10$ meV for the Coulomb interaction energy, and $T_1 = T_2 = 2$ ps for the relaxation times. For the calculations of the transient nonlinear signals we use Gaussian laser pulse envelopes $E(t)$ with a duration of 100 fs (full width at half maximum) for the pulse intensity $|E(t)|^2$; the central frequency is tuned 2 meV below the spectral position of the excitonic resonance under flat-band conditions. In the case of the time-dependent field we use laser pulses of 300 fs duration with a central frequency which is in resonance with the excitonic transition at flat band.

A. Four-wave mixing

Four-wave-mixing experiments performed in self-diffraction geometry have successfully been used to observe BO.[6,28] One advantage of this technique is that it is only weakly affected by the presence of inhomogeneous broadening, which limits the resolution of linear optical experiments. In a two-beam FWM experiment the sample is excited by two laser pulses, i.e., the optical field is given by

$$E(t) = E_1(t) \exp[-i(\mathbf{k}_1 \cdot \mathbf{r} - \omega t)]$$

$$+ E_2(t) \exp[-i(\mathbf{k}_2 \cdot \mathbf{r} - \omega t)] \quad . \tag{3}$$

Here we denote by $\mathbf{k}_1$ and $\mathbf{k}_2$ the propagation directions of the two laser pulses. $E_1(t)$ and $E_2(t)$ are the envelopes of the two pulses, which are centered at $t = 0$ and $t = \tau$, respectively. The calculated FWM signal is proportional to the square of the third-order interband polarization $|P^{(3)}(t,\tau)|^2$ in the direction $2\mathbf{k}_2 - \mathbf{k}_1$, t denotes the real time, and τ the time delay between the two pulses.[21]

Figure 1 shows calculated time-resolved FWM (TRFWM) signals, where the third-order interband polarization $|P^{(3)}(t,\tau)|^2$ is shown as a function of the real time t for different field strengths. The time delay τ was chosen to be 0. The calculated signals exhibit oscillations, which represent quantum beats induced by BO's of the optically excited carriers. Due to excitonic effects the oscillation frequency is slightly smaller than predicted from single particle theory. The exact oscil-
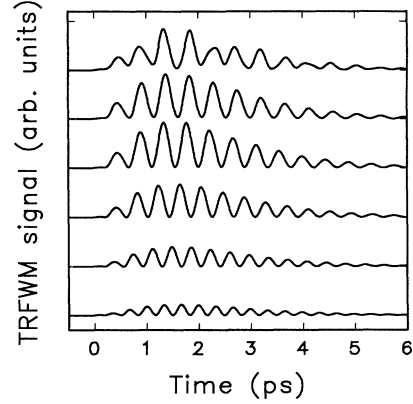

FIG. 1. Calculated time-resolved four-wave-mixing signals for electric fields $eFd = 10$ meV, 12 meV, 14 meV, 16 meV, 18 meV, and 20 meV (from top to bottom). The time delay was chosen to be 0. For further parameters see text.

lation frequency is given by the energy difference of the dominant transitions in the linear spectra, which is in the presence of excitonic effects generally somewhat smaller than the nominal WSL spacing, see Ref. 29 and the Appendix, Fig. 8. This explains why the time period of the excitonic BO, T_B^{exc}, which can be seen in Fig. 1, is slightly longer than the BO time $T_B = \frac{h}{eFd}$. This effect has recently also been discussed by Dignam et al.,[29] who have analyzed oscillations of the interband polarization in first order in the optical field.

Another signature of the Coulomb interaction in the calculated TRFWM signals is that the maximum of these signals does not appear directly after the excitation by the laser pulses around $t = 0$. The interaction-induced signal caused by the exchange terms of the Coulomb interaction, which is known to give the dominant contribution to the FWM signal in the field-free case,[21] also dominates in the case where an electric field is applied. Like in the field-free case the envelopes of the TRFWM signals show a slow rise up to a maximum and a subsequent decay, which has recently been observed experimentally.[30] The time at which the maximum appears is determined and approximately given by the dephasing time T_2.[21,31]

Figure 2 shows the calculated time-integrated FWM (TIFWM) signal, which is given by $I(\tau) = \int |P^{(3)}(t,\tau)|^2 dt$, as a function of the applied electric field. The signal oscillations, which can be seen for $eFd > 5$ meV, again represent quantum beats due to excitonic BO. The frequency of these oscillations is again determined by the energy differences in the linear spectra. The fact that the calculated TIFWM show significant signals for negative time delays again proves that FWM signals are dominated by the Coulomb interaction, i.e., that the observed quantum beats are excitonic BO (Refs. 21 and 31) (for an inhomogeneously broadened system the signals for negative time delay are suppressed due to the formation of photon echoes[12,31]).

Another interesting feature in Fig. 2 is the dependence of the signal intensity on the strength of the applied electric field. This dependence is shown in detail by the solid line in Fig. 3 where we have put the time delay equal to 0.
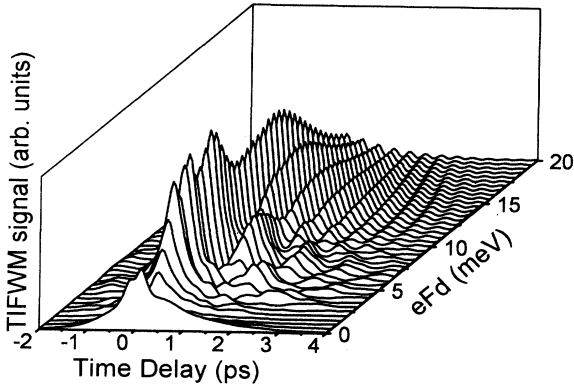
FIG. 2. Calculated time-integrated four-wave-mixing signals as function of the electric field.

We see that the signal intensity first decreases going from $eFd = 0$ to $eFd = 2$ meV. This decrease is a result of the exciton ionization induced by the applied electric field, which leads to a faster decay of the TRFWM signal and therefore to a smaller TIFWM signal. For stronger fields the intensity then increases up to values higher than the one of the field-free case. This increase, which has been observed experimentally,[32,33] can only be understood if the Coulomb exchange interaction is taken into account in the theoretical calculations. If we neglect the exchange terms in our calculations and keep only the direct Hartree terms of the Coulomb interaction,[21] we obtain the dependence of the TIFWM signal intensity given by the dashed line in Fig. 3. For WSL spacings smaller than 20 meV we see that the signal is indeed dominated by the exchange terms. The decrease of the TIFWM signal for small fields and the subsequent increase for larger fields is in agreement with experimental observation.[32,33]

For very strong electric fields, $eFd > 20$ meV, the relative importance of the contribution of the exchange terms to the signal is decreased. This can be understood to be due to the Stark localization and the nature of the ex-
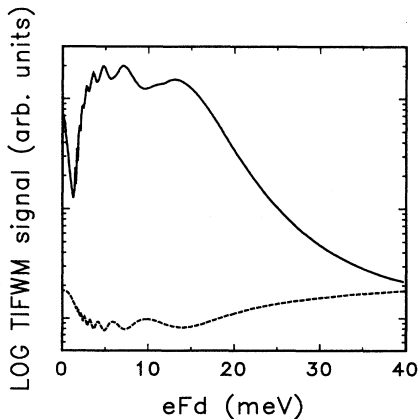

FIG. 3. Calculated time-integrated four-wave-mixing signal for time delay $\tau = 0$ as function of the electric field. Solid line, exchange contributions included; dashed line, without exchange contributions.

change terms of the on-site Coulomb interaction in our one-dimensional model. It can be shown that in the limit of very large electric fields, when the wells of the superlattice are approximately decoupled the two contributions, which can be interpreted as a renormalization of the field and the transition energy, respectively,[21,31] tend to cancel in this case.

B. Terahertz emission

In the THz emission experiment the emitted electric field caused by the coherent motion of charges in the sample is detected.[34–38] After the excitation with a short laser pulse the signal is detected using an optically gated μm-dipole antenna. This experimental technique has also successfully been used for the observation of the BO in the time domain.[7,30] Since an ideal superlattice is translationally invariant in the growth direction an intraband dipole moment, which has been used to describe the THz emission of single and double quantum-well structures in electric fields,[38] cannot be defined in this system within a k-state basis. In superlattices the current can be taken to be the source of the THz radiation. Within our model we have therefore calculated the THz signal as the derivative of the current, which is, in second order in the optical field, given by

$$E_{\text{THz}}(t) \propto \partial_t j^{(2)}(t) = \sum_{\nu=c,v} \frac{e}{\hbar} \partial_t \int \frac{\partial \epsilon_\nu(k)}{\partial k} n_\nu^{(2)}(k,t) dk \quad .$$

$$(4)$$

Within our tight-binding approach, we have neglected the so-called instantaneous contribution to the THz signal, which contributes to the signal for the duration of the optical pulse due to the fact that electron-hole pairs are created in a polarized state as a consequence of the applied electric field.[4,30]

Figure 4 shows calculated THz signals for the same electric fields as in Fig. 1, where the TRFWM signals were shown. A comparison of these two figures shows that the THz and the FWM signals have identical oscillation times, which are the excitonic BO times. In a recent publication Dignam et al.[29] calculated spectra and the time evolution of the interband polarization in first order in the optical field. They find, in agreement with the results we present here, that the excitonic BO time is generally somewhat larger than the electronic BO time. In their discussion of the oscillation range of the excitonic dipole they also apply the results of their model to the THz signal. However, the THz signal is determined by the intraband dynamics, see Eq. (4) and Refs. 12, 36, and 38. The intraband dynamics generally differs from the interband dynamics which governs the optical response. Hence, the FWM and the THz signal dynamics can exhibit significant differences. As we have discussed recently for superlattices with small miniband width the THz and the FWM signals can have different oscillations frequencies.[12] While the FWM signal showed excitonic BO, the THz emission signal was modulated with the electronic BO time. For the calculation presented in Ref.
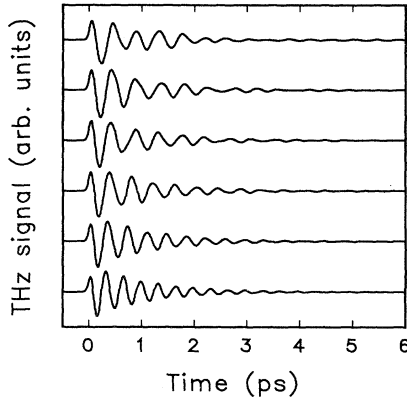
FIG. 4. Calculated terahertz emission signals for electric fields $eFd = 10$ meV, 12 meV, 14 meV, 16 meV, 18 meV, and 20 meV (from top to bottom).

12 the electric field was chosen such that the following relation was fulfilled: $T_B < T_1 = T_2 < T_B^{exc}$. Since the excitonic BO time, T_B^{exc}, was larger than the dephasing time T_2, the oscillations of the THz signal, which is given by the dynamics of the populations [see Eq. (4)] was dominated by the electronic BO time T_B. For Fig. 4, which is calculated for stronger electric fields, the relevant relation reads: $T_B < T_B^{exc} < T_1 = T_2$. Therefore now the excitonic BO time is smaller than the dephasing time and the oscillations of the THz signal are dominated by the excitonic BO time T_B^{exc}. If the exchange terms of the Coulomb interaction are neglected, or if one sets the dephasing time T_2 to smaller values then again the oscillations of the THz signal are given by the BO time T_B.

C. Dynamic localization

The effect of dynamic localization was calculated by Dunlap and Kenkre.[16] Within a tight-binding model they have analyzed the expectation value of the square of the position operator for an initially localized electron. Without an applied electric field this expectation value increases without bounds, indicating that the initially localized electron delocalizes. Also for an applied oscillating electric field, such as $F(t) = F\cos(\omega t)$, this is usually the case. Only if the amplitude and the frequency of the electric field are in a certain relation to each other, i.e., if the ratio $\frac{eFd}{\hbar\omega}$ corresponds to a root of the Bessel function J_0, then the expectation value of the square of the position operator remains bounded, and thus the electron remains localized. This phenomenon has been called dynamic localization. It was also shown that this effect strictly only appears within the tight-binding model.[16] For the case of long range intersite coupling the condition for the appearance of dynamic localization would be that the roots of the Bessel function J_0 must be spaced equidistantly, which is not the case.[16]

Later Holthaus came to similar results analyzing the problem using the Flouquet-theorem[23] and showed that

the oscillating electric field leads to a change of the effective bandwidth Δ_F as

$$\Delta_F = \left| J_0\left(\frac{eFd}{\hbar\omega}\right) \right| \Delta \quad , \qquad (5)$$

where Δ is the combined miniband width for the field-free case. Equation (5) shows that if $J_0(\frac{eFd}{\hbar\omega})$ is equal to 0 the band is flat and therefore the electrons have an infinite effective mass and are localized.

Recently there has been some discussion on specific aspects of the dynamic localization[39] in the literature, where also the influence of the Coulomb attraction between electrons and holes on this phenomenon has been considered.[40] In this paper[40] it is shown that the dynamic localization is expected to lead to an increase of the exciton binding energy and its oscillator strength in the linear optical spectrum.

In the following we want to investigate the possibility of observing dynamic localization using nonlinear optical spectroscopy in semiconductors superlattices, which is probably the most promising material system. It is clear from the aforesaid that excitonic effects and also Coulomb exchange terms have to be considered in such a theoretical investigation. We present results of calculations based on the superlattice model decribed in Sec. II, which include the oscillating electric field and Coulomb interaction in time-dependent Hartree-Fock approximation.[8] On the basis of our calculations, we propose an experiment based on THz emission spectroscopy, which should under realistic experimental conditions be able to observe the dynamic localization in semiconductor superlattices.

Figure 5 shows calculated spectra of the model superlattice as a function of $\frac{eFd}{\hbar\omega}$ for $\hbar\omega = 20$ meV. Such an electric field could experimentally be obtained, e.g., from a free-electron laser, which has been used to study photon-mediated tunneling in semiconductor superlattices.[41] The $1s$ resonance of the exciton lies energetically below the miniband continuum, which has a much smaller absorption strength than the $1s$ exciton. The spectral position of the exciton oscillates as function of $\frac{eFd}{\hbar\omega}$.[40] These oscillations are a consequence of the os-
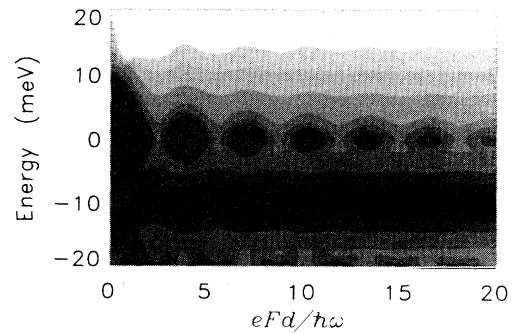

FIG. 5. Linear absorption as a function of the ratio $\frac{eFd}{\hbar\omega}$ shown as a contour plot. Dark areas indicate strong absorption. The zero of the energy scale corresponds to an optical transition to the center of the combined miniband.

cillations of the bandwidth according to Eq. (5), which can also be seen in Fig. 5. For very high $\frac{eFd}{\hbar\omega}$, the Bessel function in Eq. (5) and thus the bandwidth vanishes and therefore the line of the exciton tends to a spectral position which is situated at 10 meV, i.e., the Coulomb interaction energy V, below the center of the band.

In Fig. 6(b) we plot calculated THz emission signals for some values of the ratio $\frac{eFd}{\hbar\omega}$, and Fig. 6(a) shows the corresponding linear spectra in the vicinity of the 1s excitonic resonance. For the upper three curves the ratio is equal to 0.5, 0.8, and 1.1 and the signal exhibits oscillations with a time period which is given by the oscillation time of the oscillating electric field. A comparison of these three curves reveals that the curve for $\frac{eFd}{\hbar\omega} = 0.8$ falls off much more rapidly than the other two curves. The homogeneous linewidth of the excitonic line for this case is therefore larger compared to the other two cases [Fig. 6(a)]. This feature has nothing to do with dynamic localization and can be ascribed to the ionization of the exciton due to the action of the oscillating electric field. The fourth curve in Fig. 6(b) shows the signal for $\frac{eFd}{\hbar\omega} = 2.4$, which approximately corresponds to the first root of J_0. Due to the dynamic localization the THz signal is strongly reduced. The lower curve, for which the ratio has been increased to 4, exhibits again oscillations with a higher amplitude. In this curve one sees also that the frequency of the oscillations is no longer given by the frequency of the electric field, but is much faster. This is due to the fact that the electric field, which shifts the k vectors of the electrons across the Brillouin zone, is so strong that it leads to more than one whole transversal of the Brillouin zone per cycle of the electric field.

To demonstrate that a decrease of the signal amplitude happens whenever the ratio $\frac{eFd}{\hbar\omega}$ approaches a zero of the Bessel function J_0, we have calculated in Fig. 7 the time-integrated square of the THz signal as function of this ratio. The minima of the time-integrated signal are in excellent agreement with the first zeros of J_0, which are approximately given by 2.4, 5.5, 8.7, 11.8, 14.9, and 18.0. The first minimum in Fig. 7, which appears for $\frac{eFd}{\hbar\omega} = 0.8$ is not due to the dynamic localization but instead caused by the exciton ionization, which has been discussed before. Our calculations indicate that it should be possible to observe dynamic localization in photoexcited semiconductor superlattices using THz emission spectroscopy.
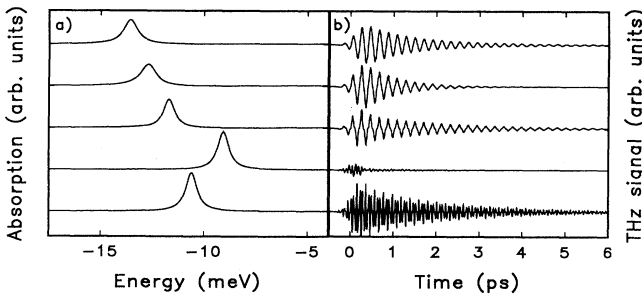

FIG. 7. Time-integrated terahertz emission signal as function of the ratio $\frac{eFd}{\hbar\omega}$.

III. CONCLUSIONS

Based on the semiconductor Bloch equations, we have presented an approach that allows the consistent calculation of linear and nonlinear coherent optical effects in semiconductors in the presence of homogeneous electric fields. We have used the extended semiconductor Bloch equations [Eqs. (1)] to calculate various linear and nonlinear optical signals of semiconductor superlattices.

For the case of a static electric field we have shown that the Coulomb exchange terms give usually the dominant contributions to the time-integrated and time-resolved four-wave-mixing signals, which therefore exhibit the same features that are well known from the field-free case,[21,31] i.e., a slow rise of the time-resolved signal and signals for negative time delays. The exchange terms are also important to explain the experimentally observed dependence[32,33] of the intensity of the four-wave-mixing signal on the strength of the electric field. Also the oscillations in terahertz emission can, depending on the ratio of the relevant times, be dominated by these Coulomb exchange terms. From the results of the calculations presented for the case of an oscillating electric field, we predict that the dynamic localization should be observable on semiconductor superlattices using terahertz emission spectroscopy.

FIG. 6. (a) Linear absorption for five values of the ratio $\frac{eFd}{\hbar\omega} = 0.5$, 0.8, 1.1, 2.4, and 4.0 (from top to bottom). (b) shows the corresponding terahertz emission signals.
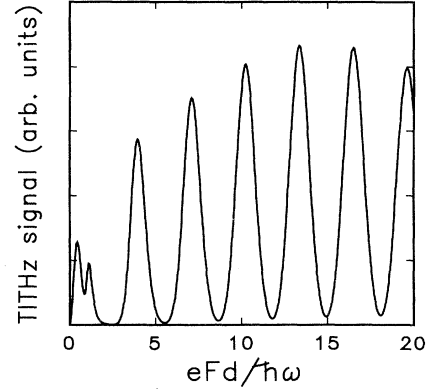
APPENDIX

Without Coulomb interaction we have the following equation of motion for the linear interband density matrix $p^{(1)}(k, t)$, see Eqs. (1):

$$\left(\partial_t - \frac{e}{\hbar}F\partial_k\right)p^{(1)}(k,t) = -\frac{i}{\hbar}\epsilon_{cv}(k)p^{(1)}(k,t)$$

$$+\mu E(t) - \frac{p^{(1)}(k,t)}{T_2} \quad . \quad (A1)$$

For excitation with an ultrashort laser pulse, i.e., $E(t) = E\delta(t - t_0)$ the solution of this equation is given in terms of Houston functions:[42]

$$p^{(1)}(k,t) = \frac{-i\mu E}{\hbar}\Theta(t - t_0)\exp\left(\frac{i}{\hbar}\int_{t_0}^{t}\epsilon_{cv}[k - \eta(t)\right.$$

$$\left.+\eta(t')]dt'\right) \quad\quad (A2)$$

with

$$\eta(t) = \frac{e}{\hbar}\int_{t_0}^{t}F(t')dt' \quad .$$

The linear polarization is given by

$$P^{(1)}(t) = \sum_k \mu^* p^{(1)}(k,t) = \int_{-\infty}^{t}\chi_0(t,t')E(t')dt' \quad . \quad (A3)$$

In the case of a static electric field and a tight-binding dispersion $\epsilon_{cv}(k) = \epsilon_0 + \frac{\Delta}{2}\cos(kd)$, Δ is the combined miniband width of the conduction and the valence band, the susceptibility reads

$$\chi_0(t,t_0) = \frac{-i|\mu|^2}{\hbar}\Theta(t - t_0)e^{i\epsilon_0(t-t_0)/\hbar}e^{(t-t_0)/T_2}$$

$$\times J_0\left[\frac{\Delta}{eFd}\sin\left(\frac{eFd}{2\hbar}(t - t_0)\right)\right] \quad . \quad (A4)$$

Using the following identity for Bessel functions, Eq. (A4) can be Fourier transformed:[43]

$$J_0(z\sin\alpha) = \sum_{l=-\infty}^{\infty} J_l^2\left(\frac{z}{2}\right)\cos(2l\alpha) \quad . \quad (A5)$$

The Fourier transformed susceptibility is given by

$$\chi_0(\omega) = \int_{-\infty}^{\infty} e^{-i\omega t}\chi_0(t,t_0)dt$$

$$= i|\mu|^2 \sum_{l=-\infty}^{\infty} J_l^2\left(\frac{\Delta}{2eFd}\right)$$

$$\times \frac{(\hbar/T_2) - i(\epsilon_0 + leFd - \hbar\omega)}{(\hbar/T_2)^2 + (\epsilon_0 + leFd - \hbar\omega)^2} \quad . \quad (A6)$$

The imaginary part of the susceptibility is proportional to the absorption. Therefore in Eq. (A6) we see that the absorption lines are energetically equidistantly spaced, which is a manifestation of the WSL. Without dephasing, i.e., for $T_2 = \infty$, the absorption lines are δ functions. Due to the dephasing, their shape becomes Lorentzian with a homogeneous linewidth given by $\frac{2\hbar}{T_2}$. If the spacing of the WSL, which is given by eFd, is larger than

the homogeneous linewidth, the WSL transitions can be resolved. (For the case of an inhomogeneously broadened system the electric field necessary for the observation of the WSL in linear spectroscopy is of course increased by the width of the inhomogeneous broadening.[44]) If the WSL spacing is smaller than the homogeneous linewidth, the WSL transitions merge, and the absorption becomes a complicated function of frequency. For small fields near the band edges Franz-Keldysh oscillations show up in the absorption, which have been observed experimentally on semiconductor superlattices.[45]

The susceptibility $\chi_0(t,t')$ satisfies a differential equation of the structure

$$L_0\chi_0(t,t') = |\mu|^2\delta(t - t') \quad , \quad\quad (A7)$$

where L_0 is a linear differential operator. For the susceptibility including the contact Coulomb potential $\chi(t,t')$ we have a differential equation, see Eqs. (1):

$$L\chi(t,t') = |\mu|^2\delta(t - t') \quad\quad\quad (A8)$$

with

$$(L - L_0) = -V \quad ,$$

here V is the contact potential.

Equation (A8) yields the following relation between χ and χ_0:[46-48]

$$\chi(t,t') = \chi_0(t,t') + \frac{V}{|\mu|^2}\int_{t'}^{t}\chi_0(t,t'')\chi(t'',t')dt'' \quad . \quad (A9)$$

This integral equation can be solved exactly by a Fourier transform:[47,48]

$$\chi(\omega) = \frac{\chi_0(\omega)}{1 - \frac{V}{|\mu|^2}\chi_0(\omega)} \quad . \quad\quad (A10)$$

Inserting the expression for χ_0, which is given in Eq. (A6), we have obtained an analytic expression for the linear absorption including the contact Coulomb potential. According to Eq. (A10), the WSL transitions are coupled together and shifted in energy due to the Coulomb interaction. Figure 8 shows a contour plot of the linear absorption as function of the WSL spacing eFd, for the
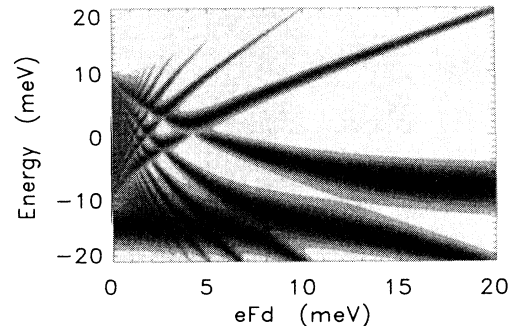

FIG. 8. Linear absorption as a function of the electric field shown as a contour plot. Dark areas indicate strong absorption. The zero of the energy scale corresponds to an optical transition to the center of the combined miniband.

same superlattice parameters which have been used for the calculations of the nonlinear signals, see Sec. II. The zero of the energy scale in Fig. 8 corresponds to an optical transition to the center of the combined miniband. For $F = 0$ the absorption is concentrated at the exciton, which is energetically situated about 4.5 meV below the lower miniband edge. For WSL spacings up to about 5 meV, Fig. 8 shows a complicated structure in the energy range of the miniband between -10 and 10 meV, which is due to both Franz-Keldysh oscillations and the WSL transitions. In the vicinity of the upper miniband edge WSL transitions are formed for $eFd > 2$ meV. Also for higher fields the absorption is concentrated in the energetically lower part of the spectrum, i.e., near the spectral position of the 1s exciton.

For WSL spacings between 3 and 10 meV, anticrossings appear in the spectrum, which have been observed experimentally on superlattices with small miniband widths.[49] These anticrossings show up whenever the excitonic 1s state comes into resonance with a WSL transition of the excitonic ionization continuum. The coupling of these states through the Coulomb potential barrier leads to this feature in the spectra. For very strong fields the central S_0 transition dominates in the spectrum. The difference of the spectral position of this transition from the center of the miniband is directly given by the Coulomb interaction energy $V = 10$ meV. The spectral positions of the resonances and their oscillator strengths are qualitatively in good agreement with calculations by Dignam and Sipe,[22] who have obtained excitonic WSL using a three-dimensional approach with variational wave functions.

[1] D.F. Blossey and P. Handler, in *Electroabsorption in Modulation Techniques*, edited by R.K. Willardson and A.C. Beer (Academic Press, New York, 1972), p. 257.

[2] E. Yablonovitch *et al.*, Phys. Rev. Lett. **63**, 976 (1989).

[3] B.B. Hu, X.-C. Chang, and D.H. Auston, Phys. Rev. Lett. **67**, 2709 (1991).

[4] S.L. Chuang *et al.*, Phys. Rev. Lett. **68**, 102 (1992).

[5] W. Sha *et al.*, Phys. Rev. Lett. **67**, 2553 (1991).

[6] J. Feldmann *et al.*, Phys. Rev. B **46**, 7252 (1992).

[7] C. Waschke *et al.*, Phys. Rev. Lett. **70**, 3319 (1993).

[8] H. Haug and S.W. Koch, *Quantum Theory of the Optical and Electronic Properties of Semiconductors*, 3rd ed. (World Scientific, Singapore, 1994), and references therein.

[9] G. von Plessen and P. Thomas, Phys. Rev. B **45**, 9185 (1992).

[10] W. Huhn and A. Stahl, Phys. Status Solidi B **124**, 167 (1984).

[11] For example, N. Peyghambarian *et al.*, Phys. Rev. Lett. **62**, 1185 (1989); K. Leo *et al.*, *ibid.* **65**, 1340 (1990).

[12] T. Meier *et al.*, Phys. Rev. Lett. **73**, 902 (1994). (Please note that some of the references in this paper were not numbered correctly. Reference 10 has to become 19 and Refs. 11–19 have to be numbered 10–18.)

[13] J. Callaway, *Quantum Theory of the Solid State* (Academic Press, New York, 1974).

[14] C. Zener, Proc. R. Soc. London Ser. A **45**, 523 (1934).

[15] W. Quade *et al.*, Phys. Rev. B **50**, 7398 (1994).

[16] D.H. Dunlap and V.M. Kenkre, Phys. Rev. B **34**, 3625 (1986).

[17] F. Bloch, Z. Phys. **52**, 555 (1928).

[18] G.H. Wannier, Phys. Rev. **117**, 432 (1960).

[19] J. Bleuse, G. Bastard, and P. Voisin, Phys. Rev. Lett. **60**, 220 (1988).

[20] H. Fukuyama, R.A. Bari, and H.C. Fogedby, Phys. Rev. B **8**, 5579 (1973).

[21] M. Lindberg, R. Binder, and S.W. Koch, Phys. Rev. A **45**, 1865 (1992).

[22] M.M. Dignam and J.E. Sipe, Phys. Rev. Lett. **64**, 1797 (1990); Phys. Rev. B **43**, 4097 (1991).

[23] M. Holthaus, Phys. Rev. Lett. **69**, 351 (1992); M. Holthaus

and D. Hone, Phys. Rev. B **47**, 6499 (1993).

[24] L. Allen and J.H. Eberly, *Optical Resonance and Two-Level Atoms* (Wiley, New York, 1975).

[25] I. Egri, Solid State Commun. **32**, 1017 (1979); J. Phys. C **15**, 461 (1982).

[26] A.M. Bouchard and M. Luban, Phys. Rev. B **47**, 6815 (1992).

[27] A. Sibille, Solid State Electron. **32**, 1455 (1989).

[28] K. Leo *et al.*, Solid State Commun. **84**, 942 (1992).

[29] M.M. Dignam, J.E. Sipe, and J. Shah, Phys. Rev. B **49**, 10 502 (1994).

[30] T. Dekorsy *et al.*, Semicond. Sci. Technol. **9**, 1959 (1994).

[31] M. Wegener *et al.*, Phys. Rev. A **42**, 5675 (1990); F. Jahnke *et al.*, Phys. Rev. B **50**, 8114 (1994).

[32] J. Feldmann (private communication).

[33] P. Leisching *et al.*, Phys. Rev. B **50**, 14 389 (1994).

[34] X.-C. Zhang *et al.*, Appl. Phys. Lett. **56**, 1011 (1990); **56**, 2228 (1990).

[35] P.C.M. Planken *et al.*, Appl. Phys. Lett. **61**, 2009 (1992).

[36] P.C.M. Planken *et al.*, Phys. Rev. Lett. **69**, 3800 (1992).

[37] H.G. Roskos *et al.*, Phys. Rev. Lett. **68**, 2216 (1992).

[38] M.S.C. Luo *et al.*, IEEE J. Quantum Electron. **30**, 1478 (1994).

[39] For example, X.-G. Zhao, Phys. Lett. A **167**, 291 (1992); Y.O. Averkov *et al.*, Phys. Rev. B **48**, 17 995 (1993); J. Zak, Phys. Rev. Lett. **71**, 2623 (1993); X.-G. Zhao, J. Phys. Condens. Matter **6**, 2751 (1994).

[40] P. Ray and P.K. Basu, Phys. Rev. B **50**, 14 595 (1994).

[41] P.S.S. Guimaraes *et al.*, Phys. Rev. Lett. **70**, 3792 (1993).

[42] W.V. Houston, Phys. Rev. **57**, 185 (1940).

[43] I.M. Ryshik and I.S. Gradstein, *Summen-, Produkt- und Integraltafeln* (VEB Deutscher Verlag der Wissenschaften, Berlin, 1963).

[44] G. von Plessen *et al.*, Phys. Rev. B **49**, 14 058 (1994).

[45] S. Niki *et al.*, Appl. Phys. Lett. **56**, 475 (1990).

[46] S. Schmitt-Rink *et al.*, Opt. Lett. **15**, 60 (1990).

[47] D.S. Chemla *et al.*, Phys. Status Solidi B **159**, 11 (1990).

[48] M. Kleber, Phys. Rep. **236**, 331 (1994).

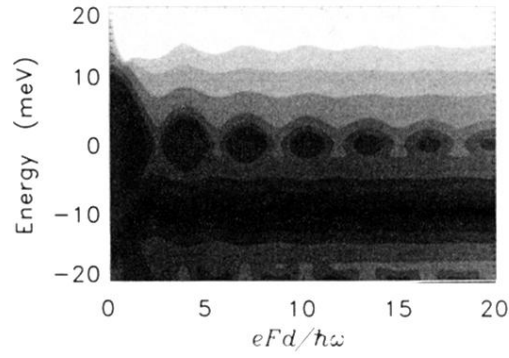[49] A.M. Fox *et al.*, Phys. Rev. B **46**, 15 365 (1992).

FIG. 5. Linear absorption as a function of the ratio $\frac{eFd}{\hbar\omega}$ shown as a contour plot. Dark areas indicate strong absorption. The zero of the energy scale corresponds to an optical transition to the center of the combined miniband.
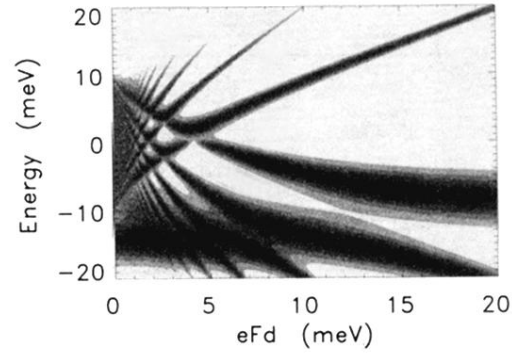
FIG. 8. Linear absorption as a function of the electric field shown as a contour plot. Dark areas indicate strong absorption. The zero of the energy scale corresponds to an optical transition to the center of the combined miniband.